

Cite this: *J. Mater. Chem. A*, 2021, 9, 7190Binding and separation of CO<sub>2</sub>, SO<sub>2</sub> and C<sub>2</sub>H<sub>2</sub> in homo- and hetero-metallic metal–organic framework materials†Lydia Briggs,<sup>‡a</sup> Ruth Newby,<sup>‡b</sup> Xue Han,<sup>a</sup> Christopher G. Morris,<sup>ac</sup> Mathew Savage,<sup>id a</sup> Cristina Perez Krap,<sup>b</sup> Timothy L. Eason,<sup>id d</sup> Mark D. Frogley,<sup>id c</sup> Gianfelice Cinque,<sup>id c</sup> Claire A. Murray,<sup>c</sup> Chiu C. Tang,<sup>c</sup> Junliang Sun,<sup>id e</sup> Sihai Yang<sup>id \*a</sup> and Martin Schröder<sup>id \*a</sup>

We report the adsorption of C<sub>2</sub>H<sub>2</sub>, CO<sub>2</sub> and SO<sub>2</sub> in a new, ultra-stable Cr(III)-based MOF, MFM-300(Cr), {[Cr<sub>2</sub>(OH)<sub>2</sub>(L)], H<sub>4</sub>L = biphenyl-3,3',5,5'-tetracarboxylic acid}. MFM-300(Cr) shows uptakes of 7.37, 7.73 and 8.59 mmol g<sup>-1</sup> for CO<sub>2</sub>, C<sub>2</sub>H<sub>2</sub> and SO<sub>2</sub>, respectively, at 273 K, 1.0 bar, and shows a higher selectivity for SO<sub>2</sub>/CO<sub>2</sub> compared with the Al(III) analogue MFM-300(Al) (selectivity of 79 vs. 45). In order to monitor the effects of changing metal centre on gas uptake and to integrate the properties of the homometallic analogues, the mixed metal MFM-300(Al<sub>0.67</sub>Cr<sub>0.33</sub>), [Al<sub>1.34</sub>Cr<sub>0.66</sub>(OH)<sub>2</sub>(L)] has been synthesised. *In situ* synchrotron micro-FTIR spectroscopy has identified distinct CO<sub>2</sub> binding environments on Al–O(H)–Al, Cr–O(H)–Cr and Al–O(H)–Cr bridges in MFM-300(Al<sub>0.67</sub>Cr<sub>0.33</sub>), and we have determined the binding domains for these gases by *in situ* synchrotron X-ray diffraction in both MFM-300(Cr) and MFM-300(Al<sub>0.67</sub>Cr<sub>0.33</sub>). The capability of these materials for gas separation has been confirmed by dynamic breakthrough experiments. The incorporation of Al(III) and Cr(III) within the same framework allows tuning of the host–guest and guest–guest interactions within these functional porous materials.

Received 24th January 2021  
Accepted 15th February 2021

DOI: 10.1039/d1ta00687h

rsc.li/materials-a

High porosity, chemical and thermal stability and flexible design are critical features of metal–organic framework (MOF) materials. Design-led incorporation of functional groups such as hydroxyl (–OH),<sup>1–3</sup> amine (–NH<sub>2</sub>)<sup>4,5</sup> and halogen (–F, –Cl, –Br)<sup>6–8</sup> groups to form supramolecular interactions with guest species is an effective methodology for enhancing gas sorption.<sup>9,10</sup> The design of MOFs with open metal sites has been explored widely, but this can often lead to materials that are unstable upon desolvation and/or in contact with moisture.<sup>11,12</sup>

Variation of metal centres in complex structures is a methodology that may alter or enhance materials properties but does not necessarily introduce significant structural changes.<sup>13</sup> We were thus interested to investigate the properties of mixed-metal MOF materials, and chose Al(III) and Cr(III) as target centres to compare within the MFM-300 series.

Cr(III)-Based MOFs tend to be highly stable and have been used in catalysis.<sup>14</sup> MIL-101(Cr) has removable terminal water molecules connected to a trinuclear [Cr<sub>3</sub>(μ<sub>3</sub>-O)(O<sub>2</sub>CR)<sub>6</sub>(–F,OH)(H<sub>2</sub>O)<sub>2</sub>] building block, leaving two Lewis acidic sites accessible to catalyse a range of reactions such as oxidations and epoxidations.<sup>15–17</sup> Its extensive use can be attributed to the stability of MIL-101(Cr) to water, and Cr(III)-based MOFs generally show enhanced chemical stability as a result of the low lability of Cr(III), which can also be exploited for gas sorption.<sup>18,19</sup> The Al(III)-tetracarboxylate MOF, MFM-300(Al), shows high adsorption of CO<sub>2</sub> and SO<sub>2</sub>,<sup>2</sup> while heterometallic MOFs with multiple metal centres within the same framework can show enhanced gas sorption and catalytic capabilities.<sup>20,21</sup> Herein, we report the synthesis and gas adsorption of two new Cr-containing analogues of MFM-300(Al): the homometallic MFM-300(Cr) and the mixed metal analogue MFM-300(Al<sub>0.67</sub>Cr<sub>0.33</sub>). Their capability for gas separation has been studied by IAST analysis<sup>22</sup> and by dynamic breakthrough experiments. Synchrotron X-ray powder diffraction has been

<sup>a</sup>School of Chemistry, University of Manchester, Oxford Road, Manchester, M13 9PL, UK. E-mail: Sihai.Yang@manchester.ac.uk; M.Schroder@manchester.ac.uk<sup>b</sup>School of Chemistry, University of Nottingham, University Park, Nottingham, NG7 2RD, UK<sup>c</sup>Diamond Light Source, Harwell Science Campus, Oxfordshire, OX11 0DE, UK<sup>d</sup>School of Chemistry, Cardiff University, Cardiff, CF10 3AT, UK<sup>e</sup>College of Chemistry and Molecular Engineering, Peking University, Beijing, 100871, China† Electronic supplementary information (ESI) available: Synthesis procedures, characterization, and additional analysis of crystal structures. Structural data of MFM-300(Al<sub>1–x</sub>Cr<sub>x</sub>) (x = 0, 0.33, 1) derived from powder X-ray diffraction. CCDC 1952013, 1952268, 1952287 and 1952276 for activated MFM-300(Al<sub>0.67</sub>Cr<sub>0.33</sub>), CO<sub>2</sub>, C<sub>2</sub>H<sub>2</sub>- and SO<sub>2</sub>-loaded structures, respectively, and 1952277, 1952321, 1952320 and 1952280 for activated MFM-300(Cr), CO<sub>2</sub>, C<sub>2</sub>H<sub>2</sub>, and SO<sub>2</sub>-loaded structures, respectively. For ESI and crystallographic data in CIF or other electronic format see DOI: 10.1039/d1ta00687h

‡ These authors contributed equally to the work.



used to determine the preferred binding sites for adsorbed CO<sub>2</sub>, SO<sub>2</sub> and C<sub>2</sub>H<sub>2</sub> within these materials, and synchrotron micro-IR spectroscopy confirms intermolecular interactions of adsorbed gas molecules with M-μ<sub>2</sub>O(H)-M' (M and M' = Al or Cr) functionalities. This study reveals new insights into the effects of partial transmetalation in isostructural MOFs on host-guest interactions and overall gas adsorption capacity.

## Results and discussion

MFM-300(Cr) was synthesised by hydrothermal reaction of H<sub>4</sub>L (biphenyl-3-3'-5-5'-tetracarboxylic acid) and CrCl<sub>3</sub>·6H<sub>2</sub>O in acidic (HCl) water, and was isolated as blue, microcrystalline powder (yield = 91%). High resolution synchrotron X-ray diffraction confirms that MFM-300(Cr) possesses extended metal chains of [CrO<sub>4</sub>(OH)<sub>2</sub>] bridged by L<sup>4-</sup> and two *cis*-μ<sub>2</sub>-OH groups forming 1D channels that propagate along the *c* axis. The heterometallic MFM-300(Al<sub>1-x</sub>Cr<sub>x</sub>) was synthesised *via* a similar method but using both Al and Cr salts in the reaction to give a light blue microcrystalline powder (yield ~ 86%). Various ratios of Al and Cr salts were tested for synthesis, and the actual Al : Cr ratio within the heterometallic product was determined by ICP-OES analysis (see ESI†). Among all the obtained materials with different ratios, MFM-300(Al<sub>0.67</sub>Cr<sub>0.33</sub>) shows the best performance in terms of gas sorption. MFM-300(Al<sub>0.67</sub>Cr<sub>0.33</sub>) is isostructural to the parent complexes MFM-300(M) (M = Al, Cr) (Table S3†), with M-OH bond distances of 1.930(1) Å, 1.953(1) Å and 1.868(5) Å in MFM-300(Al), MFM-

300(Cr) and MFM-300(Al<sub>0.67</sub>Cr<sub>0.33</sub>), respectively. The homogeneity of the distribution of Cr and Al in MFM-300(Al<sub>0.67</sub>Cr<sub>0.33</sub>) has been studied by synchrotron FT-IR experiments. Three bands for ν(OH) are observed at 3690, 3672, and 3641 cm<sup>-1</sup> assigned to Al-(OH)-Al, Al-(OH)-Cr and Cr-(OH)-Cr moieties, respectively, thus demonstrating a homogeneous distribution of M(III) centres (Fig. 1d). The ratio of Al : Cr is further confirmed by TGA (Fig. S1†).

Desolvated MFM-300(Cr) and MFM-300(Al<sub>0.67</sub>Cr<sub>0.33</sub>) show similar BET surface areas of 1360 and 1305 m<sup>2</sup> g<sup>-1</sup>, respectively, and adsorption isotherms for CO<sub>2</sub>, C<sub>2</sub>H<sub>2</sub> and SO<sub>2</sub> were measured for these materials. At 273 K and 1.0 bar, the total gas uptakes for MFM-300(Al), MFM-300(Cr) and MFM-300(Al<sub>0.67</sub>Cr<sub>0.33</sub>) are 7.00, 8.48 and 7.37 mmol g<sup>-1</sup> for CO<sub>2</sub>, 6.89, 8.67 and 7.73 mmol g<sup>-1</sup> for C<sub>2</sub>H<sub>2</sub>, and 8.1, 10.0 and 8.59 mmol g<sup>-1</sup> for SO<sub>2</sub>, respectively (Fig. 1a-c). Taking the difference in molecular mass per unit cell into account, the number of gas molecules per metal ion in each MOF is given Table S10.† The thermodynamic parameters *Q*<sub>st</sub> and Δ*S* were calculated using the van't Hoff isochore (Fig. S6-S11†). With CO<sub>2</sub>, C<sub>2</sub>H<sub>2</sub> and SO<sub>2</sub> loadings between 0.5-4.0 mmol g<sup>-1</sup>, the values of *Q*<sub>st</sub> are 25.5-28.6, 35.0-42.8 and 39.3-46.0 kJ mol<sup>-1</sup> for MFM-300(Cr); and 26.4-29.3, 31.5-32.0 and 43.5-54.6 kJ mol<sup>-1</sup> for MFM-300(Al<sub>0.67</sub>Cr<sub>0.33</sub>), which are similar to those of MFM-300(Al).<sup>1,2</sup> Ten cycles of adsorption/desorption of SO<sub>2</sub> were conducted for all three materials at 298 K between 0-0.1 bar, and all maintained their full adsorption capacity, confirming their excellent stability under these conditions (Fig. 2a-c). Throughout the

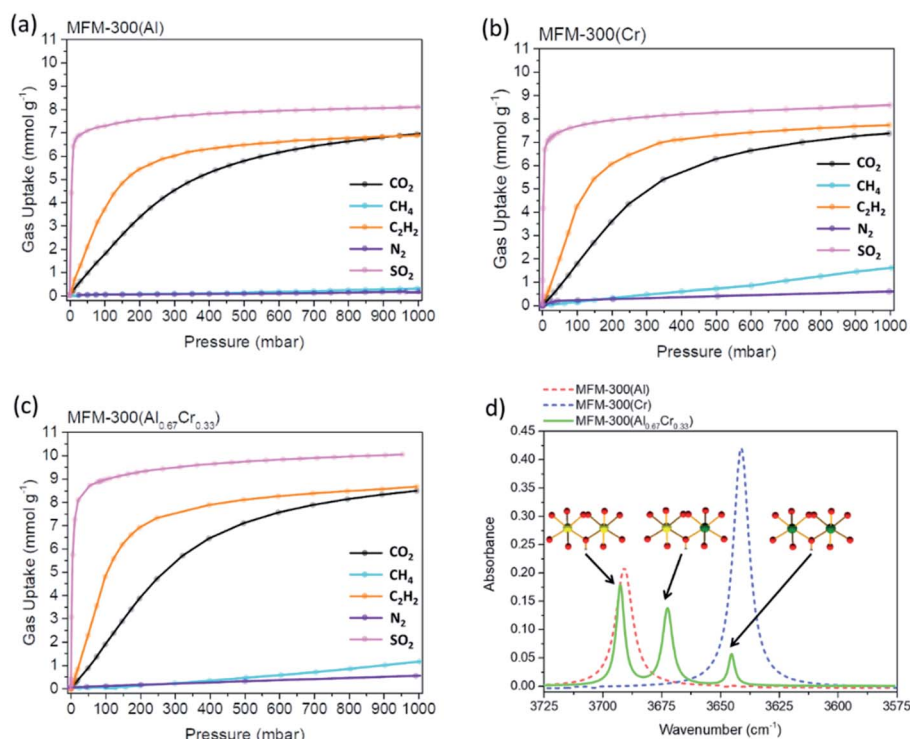


Fig. 1 Adsorption isotherms of CO<sub>2</sub> (black), CH<sub>4</sub> (aqua), C<sub>2</sub>H<sub>2</sub> (orange), N<sub>2</sub> (purple) and SO<sub>2</sub> (pink) in (a) MFM-300(Al), (b) MFM-300(Cr) and (c) MFM-300(Al<sub>0.67</sub>Cr<sub>0.33</sub>), at 273 K, 0–1 bar; (d) FT-IR spectrum showing the ν(OH) peak in the M-OH-M functionality in MFM-300(Al) (red), MFM-300(Al<sub>0.67</sub>Cr<sub>0.33</sub>) (green) and MFM-300(Cr) (blue).



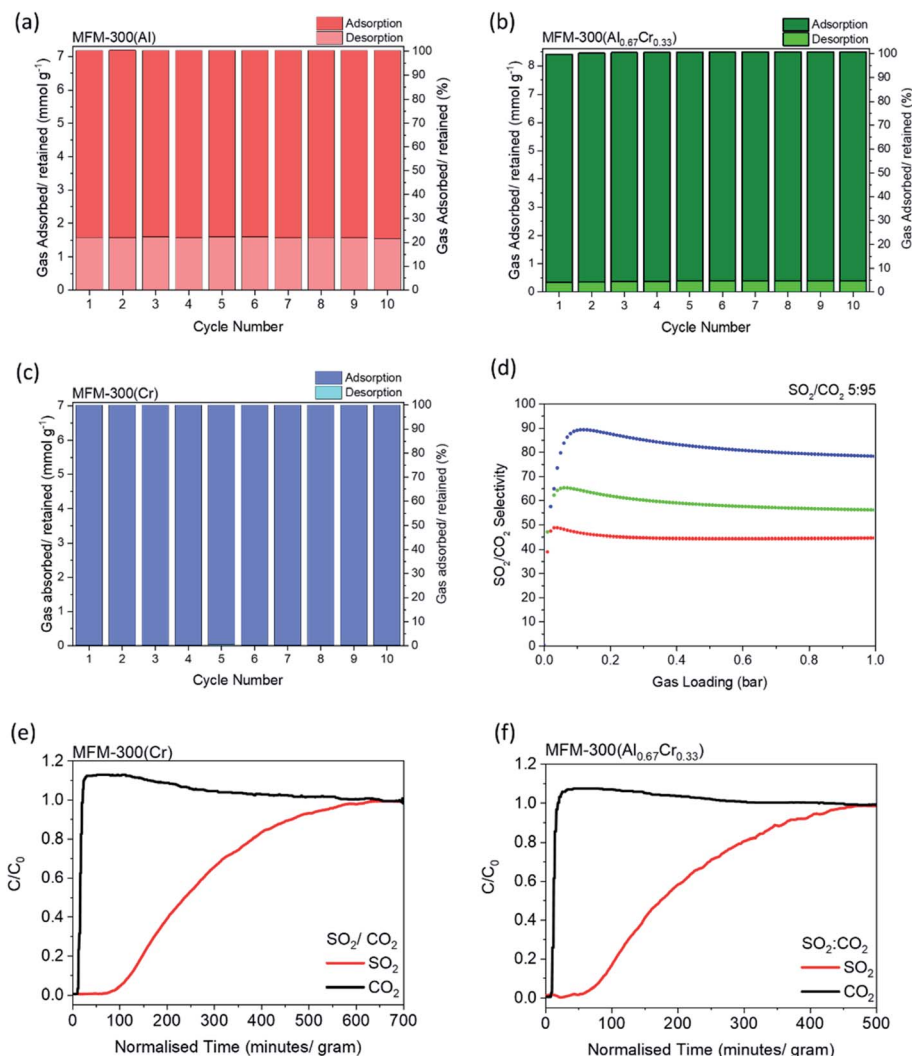


Fig. 2 Cycling experiments of  $\text{SO}_2$  at 298 K between 0–0.1 bar in (a) MFM-300(Al), (b) MFM-300( $\text{Al}_{0.67}\text{Cr}_{0.33}$ ) and (c) MFM-300(Cr). (d) IAST selectivity of  $\text{SO}_2/\text{CO}_2$  (5 : 95) in MFM-300(Al) (red), MFM-300( $\text{Al}_{0.67}\text{Cr}_{0.33}$ ) (green) and MFM-300(Cr) (blue) up to 1 bar at 273 K. Breakthrough plots for  $\text{SO}_2/\text{CO}_2$  (0.4%  $\text{SO}_2$ , 16%  $\text{CO}_2$ ) diluted in He through a fixed bed packed with (e) MFM-300(Cr) and (f) MFM-300( $\text{Al}_{0.67}\text{Cr}_{0.33}$ ) at 298 K and 1 bar.

cycles, MFM-300(Al) and MFM-300( $\text{Al}_{0.67}\text{Cr}_{0.33}$ ) were found to retain  $\text{SO}_2$  upon desorption under dynamic vacuum at 298 K (22% and 5%  $\text{SO}_2$  retained, respectively), and require elevated temperature to fully remove  $\text{SO}_2$ . In contrast, MFM-300(Cr) shows negligible retention of  $\text{SO}_2$  (<0.4% or <0.05  $\text{mmol g}^{-1}$ ) under dynamic vacuum at ambient temperature. Combined with its high structural stability and adsorption capacity, MFM-300(Cr) offers a regenerable platform for  $\text{SO}_2$  capture of relevance to flue gas desulfurization.<sup>23–25</sup> We further explored these MOFs for the separation of  $\text{SO}_2$  from  $\text{CO}_2$ , as  $\text{SO}_2$  is an important flue gas impurity in  $\text{CO}_2$  streams and can lead to numerous operational problems in carbon separation and geological sequestration.<sup>26,27</sup> IAST selectivities of  $\text{SO}_2/\text{CO}_2$  (5 : 95) were calculated for these MOFs from pure component isotherms between 0–1 bar at 273 K (Fig. 2d). Notably, MFM-300(Cr) shows the highest  $\text{SO}_2/\text{CO}_2$  selectivity of 79 at 273 K and 1 bar compared to 56 for MFM-300( $\text{Al}_{0.67}\text{Cr}_{0.33}$ ) and 45 for MFM-

300(Al). Dynamic breakthrough experiments with 0.4%  $\text{SO}_2$  and 16%  $\text{CO}_2$  in He also confirmed the selective retention of low concentrations of  $\text{SO}_2$  with MFM-300(Cr) and MFM-300( $\text{Al}_{0.67}\text{Cr}_{0.33}$ ) under flow conditions (Fig. 2e and f). In both cases,  $\text{CO}_2$  eluted first and saturated rapidly [ $t = 19$  and 21  $\text{min g}^{-1}$  for MFM-300( $\text{Al}_{0.67}\text{Cr}_{0.33}$ ) and MFM-300(Cr), respectively], whereas  $\text{SO}_2$  starts to elute at  $t = 56$  and 76  $\text{min g}^{-1}$ , respectively, and shows a steadier breakthrough curve.

To gain deeper understanding of the host–guest interactions underpinning these processes and to rationalise the observed gas selectivities, *in situ* high resolution synchrotron PXRD has been used to determine the preferred binding sites for  $\text{CO}_2$ ,  $\text{SO}_2$  and  $\text{C}_2\text{H}_2$  molecules within MFM-300(Cr) and MFM-300( $\text{Al}_{0.67}\text{Cr}_{0.33}$ ) *via* Rietveld refinement (Fig. 3–5; Tables S1 and S2†). For  $\text{CO}_2$ , the primary site of adsorption,  $\text{CO}_2^{\text{I}}$ , is bound to the  $\mu_2$ -OH group of the hydroxyl-metal chain,  $\text{O}^{\mu_2\text{-OH}}\dots\text{O}^{\text{CO}_2} = 3.301(4)$ , 3.39(1), 3.21(3) Å for MFM-300(Cr), MFM-



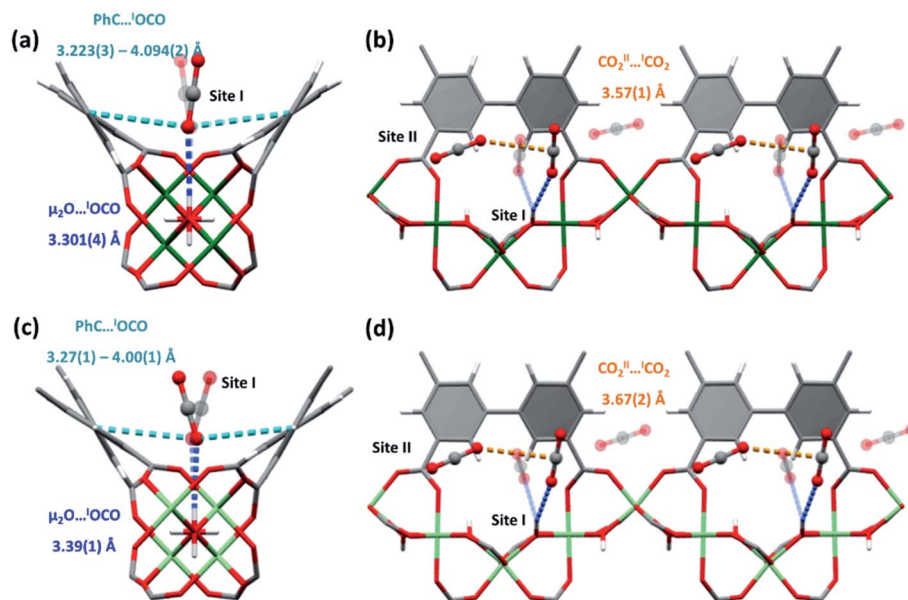


Fig. 3 Views of binding pocket of CO<sub>2</sub><sup>I</sup> and CO<sub>2</sub><sup>I</sup>...CO<sub>2</sub><sup>II</sup> interactions in (a and b) MFM-300(Cr) and (c and d) MFM-300(Al<sub>0.67</sub>Cr<sub>0.33</sub>). Positionally disordered molecules are shown as translucent. Green: Cr, Light green: AlCr, red: O, grey: C, white: H. Blue bond: μ<sub>2</sub>-OH...CO<sub>2</sub><sup>I</sup>, turquoise bond: Ph...CO<sub>2</sub><sup>I</sup>, orange bonds: CO<sub>2</sub><sup>I</sup>...CO<sub>2</sub><sup>II</sup> interactions.

300(Al<sub>0.67</sub>Cr<sub>0.33</sub>) and MFM-300(Al),<sup>2</sup> respectively, and is disordered by a mirror plane that dissects the μ<sub>2</sub>-OH (Fig. 4).<sup>28,29</sup> CO<sub>2</sub><sup>I</sup> is further enclosed by aromatic C–H groups of the biphenyl core of the linker and forms additional supramolecular interactions [O<sup>CO<sub>2</sub><sup>I</sup></sup>...C<sup>Aromatic</sup> = 3.223(3)–4.094(2) Å in MFM-300(Cr) and 3.27(1)–4.00(1) Å in MFM-300(Al<sub>0.67</sub>Cr<sub>0.33</sub>)]. The second site, CO<sub>2</sub><sup>II</sup>, is positioned near-perpendicular to CO<sub>2</sub><sup>I</sup> with full occupancy. The C<sup>CO<sub>2</sub><sup>I</sup></sup>...O<sup>CO<sub>2</sub><sup>II</sup></sup> distances in MFM-300(Cr), MFM-300(Al<sub>0.67</sub>Cr<sub>0.33</sub>) and MFM-300(Al) are 3.57(1), 3.67(2) and 3.92(1) Å, respectively, suggesting a more compact packing of CO<sub>2</sub> in MFM-300(Cr).

For SO<sub>2</sub>, two adsorption sites were observed in both MFM-300(Cr) and MFM-300(Al<sub>0.67</sub>Cr<sub>0.33</sub>) (Fig. 4). As for CO<sub>2</sub>, the primary SO<sub>2</sub> site, SO<sub>2</sub><sup>I</sup>, is located with an end-on mode to the bridging μ<sub>2</sub>-OH group, O<sup>μ<sub>2</sub>-OH</sup>...O<sup>SO<sub>2</sub></sup> = 3.350(6), 3.163(1) and 3.201(6) Å in MFM-300(Cr), MFM-300(Al<sub>0.67</sub>Cr<sub>0.33</sub>) and MFM-300(Al) respectively. SO<sub>2</sub><sup>I</sup> also interacts with the surrounding linker moieties *via* van der Waals interactions [O<sup>SO<sub>2</sub><sup>I</sup></sup>...C<sup>Aromatic</sup> = 3.08(2)–4.26(7) Å in MFM-300(Cr) and 3.055(2)–3.688(3) Å in MFM-300(Al<sub>0.67</sub>Cr<sub>0.33</sub>)]. SO<sub>2</sub> at site II is located perpendicularly to SO<sub>2</sub><sup>I</sup> with the S<sup>SO<sub>2</sub><sup>I</sup></sup>...O<sup>SO<sub>2</sub><sup>II</sup></sup> distances being 3.45(3), 3.477(7) and 3.34(7) Å for MFM-300(Cr), MFM-300(Al<sub>0.67</sub>Cr<sub>0.33</sub>) and

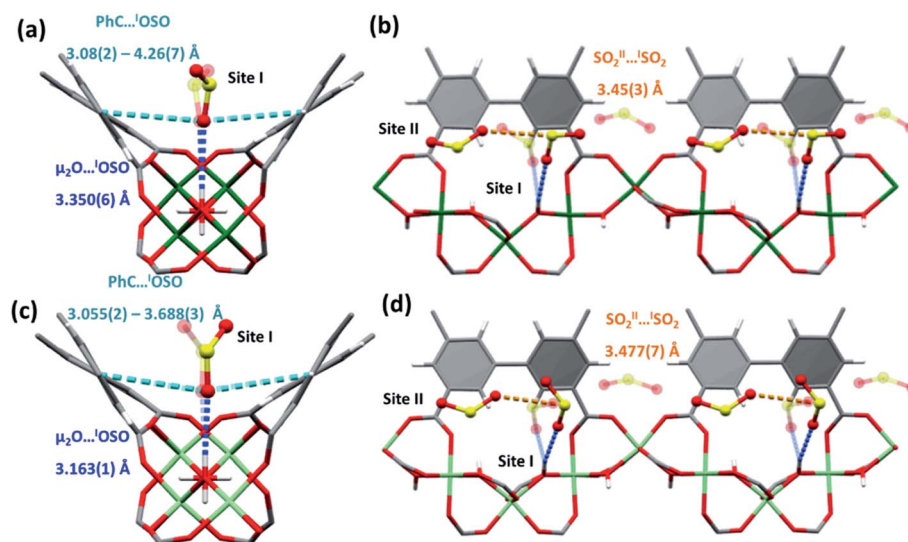


Fig. 4 Views of binding of SO<sub>2</sub><sup>I</sup> and of SO<sub>2</sub><sup>I</sup>...SO<sub>2</sub><sup>II</sup> interactions in (a and b) MFM-300(Cr) and (c and d) MFM-300(Al<sub>0.67</sub>Cr<sub>0.33</sub>). Positionally disordered molecules are shown as translucent. Green: Cr, light green: AlCr, yellow: S, red: O, grey: C, white: H. Blue bond: μ<sub>2</sub>-OH...OSO<sup>I</sup>, turquoise bond: Ph...SO<sub>2</sub><sup>I</sup>, orange bonds: SO<sub>2</sub><sup>I</sup>...SO<sub>2</sub><sup>II</sup> interactions.



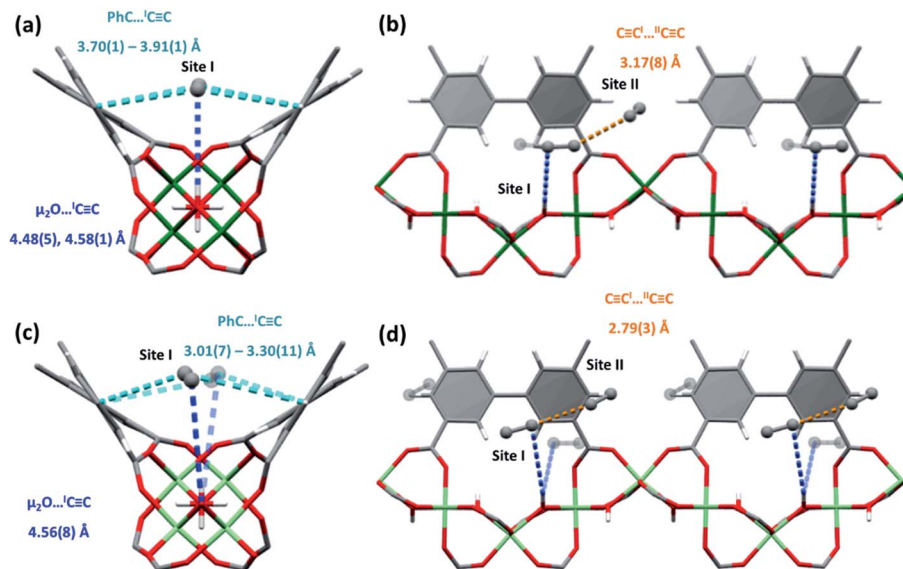


Fig. 5 Views of binding of C<sub>2</sub>H<sub>2</sub><sup>I</sup> and of C<sub>2</sub>H<sub>2</sub><sup>I</sup>...C<sub>2</sub>H<sub>2</sub><sup>II</sup> interactions in (a and b) MFM-300(Cr) and (c and d) MFM-300(Al<sub>0.67</sub>Cr<sub>0.33</sub>). Positionally disordered molecules are shown as translucent. Green: Cr, light green: AlCr, red: O, grey: C, white: H. Blue bond: μ<sub>2</sub>-OH...C≡C<sup>I</sup>, turquoise bond: Ph...C≡C<sup>I</sup>, orange bonds: C≡C<sup>I</sup>...C≡C<sup>II</sup> interactions.

MFM-300(Al), respectively. SO<sub>2</sub><sup>II</sup> also shows weak interactions with the phenyl ring of linker with S<sup>SO<sub>2</sub></sup>...C<sup>Aromatic</sup> = 3.53(1) and 3.445(3) Å, for MFM-300(Cr) and MFM-300(Al<sub>0.67</sub>Cr<sub>0.33</sub>), respectively.

As the bonding distances usually reflect the strength of the host-guest and guest-guest interactions within these system, which often influences the gas selectivities, a summary of bonding distances in CO<sub>2</sub> and SO<sub>2</sub>-loaded MFM-300(Cr), MFM-300(Al<sub>0.67</sub>Cr<sub>0.33</sub>) and MFM-300(Al) is shown in Table 1. When comparing the two single-metal MOFs, MFM-300(Cr) shows weaker bonding interaction to both CO<sub>2</sub> and SO<sub>2</sub> (longer bonding distances) than MFM-300(Al). This reconciles the observed differences in SO<sub>2</sub> residues within these two materials upon desorption at ambient temperature. However, the strong interactions with both CO<sub>2</sub> and SO<sub>2</sub> means that MFM-300(Al) achieves a lower IAST selectivity. The hetero-metallic MFM-300(Al<sub>0.67</sub>Cr<sub>0.33</sub>) exhibits the weakest binding to CO<sub>2</sub> and the strongest binding to SO<sub>2</sub> among these three MOFs. However, the IAST selectivity of SO<sub>2</sub>/CO<sub>2</sub> in MFM-300(Al<sub>0.67</sub>Cr<sub>0.33</sub>) falls in between that of the two single-metal MOFs. This strongly suggests that the host-guest bonding distance is not the sole factor to affect the observed selectivity, which will also be influenced by guest-guest interactions. Also, MFM-300(Al<sub>0.67</sub>Cr<sub>0.33</sub>) has a slightly enlarged pore diameter compared

to MFM-300(Al) due to doping with Cr(III), which also likely contributes to the slightly higher gas uptake. In addition, doping MFM-300(Al) with Cr(III) may well form defects leading to increased porosity and additional binding and interaction sites. CO<sub>2</sub> exhibits most compact packing in MFM-300(Cr) (shorter CO<sub>2</sub>...CO<sub>2</sub> distance), whereas SO<sub>2</sub> packs most tightly in MFM-300(Al).

For C<sub>2</sub>H<sub>2</sub>, two distinct positions of C<sub>2</sub>H<sub>2</sub> were observed with both MFM-300(Cr) and MFM-300(Al<sub>0.67</sub>Cr<sub>0.33</sub>) (Fig. 5). C<sub>2</sub>H<sub>2</sub><sup>I</sup> interacts with the bridging hydroxyl group of MFM-300(Cr) in a side-on manner, and in MFM-300(Al<sub>0.67</sub>Cr<sub>0.33</sub>), C<sub>2</sub>H<sub>2</sub><sup>I</sup> is slightly off-perpendicular. In both cases, the interactions between the H atom of the hydroxyl to the electron rich π C≡C in C<sub>2</sub>H<sub>2</sub> are weaker than that of CO<sub>2</sub> and SO<sub>2</sub> systems, with longer bonding distances being observed [HO...C<sup>C<sub>2</sub>H<sub>2</sub><sup>I</sup></sup> = 4.48(5)–4.58(1) Å and 4.56(8) Å in MFM-300(Cr) and MFM-300(Al<sub>0.67</sub>Cr<sub>0.33</sub>), respectively]. C<sub>2</sub>H<sub>2</sub><sup>I</sup> is further anchored within a pocket through π...π stacking interactions with the adjacent phenyl core of the linkers [C<sup>C<sub>2</sub>H<sub>2</sub><sup>I</sup></sup>...C<sup>Aromatic</sup> = 3.51(2), 3.73(2), 3.91(1) Å in MFM-300(Cr) and 3.01(7), 3.30(11) Å in MFM-300(Al<sub>0.67</sub>Cr<sub>0.33</sub>)]. C<sub>2</sub>H<sub>2</sub><sup>II</sup> interacts *via* dipole interactions with C<sub>2</sub>H<sub>2</sub><sup>I</sup> in a T-shape orientation in MFM-300(Cr) [C<sup>C<sub>2</sub>H<sub>2</sub><sup>I</sup></sup>...C<sup>C<sub>2</sub>H<sub>2</sub><sup>II</sup></sup> = 3.17(8) Å], and is more skewed in MFM-300(Al<sub>0.67</sub>Cr<sub>0.33</sub>) but with shorter intermolecular distances [C<sup>C<sub>2</sub>H<sub>2</sub><sup>I</sup></sup>...C<sup>C<sub>2</sub>H<sub>2</sub><sup>II</sup></sup> = 2.79(3) Å].

Table 1 Summary of bonding distances within CO<sub>2</sub> and SO<sub>2</sub>-loaded MFM-300(Cr), MFM-300(Al<sub>0.67</sub>Cr<sub>0.33</sub>) and MFM-300(Al)

Bonding distance (Å)	MFM-300(Cr)	MFM-300(Al <sub>0.67</sub> Cr <sub>0.33</sub> )	MFM-300(Al)
O <sup>μ<sub>2</sub>-OH</sup> ...O <sup>CO<sub>2</sub></sup>	3.301(4)	3.39(1)	3.21(3)
O <sup>μ<sub>2</sub>-OH</sup> ...O <sup>SO<sub>2</sub></sup>	3.350(6)	3.163(1)	3.201(6)
O <sup>CO<sub>2</sub><sup>I</sup></sup> ...O <sup>CO<sub>2</sub><sup>II</sup></sup>	3.57(1)	3.67(2)	3.92(1)
O <sup>SO<sub>2</sub></sup> ...O <sup>SO<sub>2</sub><sup>II</sup></sup>	3.45(3)	3.477(7)	3.34(7)



The position of  $C_2H_2^H$  is further stabilised by weak van der Waals interactions with the phenyl core of the adjacent linker moieties [ $C^{C_2H_2^H} \dots C^{Aromatic} = 3.97(4)$ ,  $4.35(7)$  Å and  $3.29(13)$ ,  $3.52(19)$  Å for MFM-300(Cr) and MFM-300( $Al_{0.67}Cr_{0.33}$ ), respectively]. Thus, both MOFs have strong affinity to  $C_2H_2$  through the combined numerous weak interactions which leads to the efficient packing of  $C_2H_2$  within the pores and high  $C_2H_2$  uptake.

To study the dynamics of host-guest binding, *in situ* synchrotron micro-IR spectroscopy was undertaken on MFM-300(Al), MFM-300(Cr) and MFM-300( $Al_{0.67}Cr_{0.33}$ ) as a function of  $CO_2$  loading (Fig. 6). Upon activation under a flow of He, bands for the  $\nu(OH)$  stretching modes were observed at  $3690\text{ cm}^{-1}$  and  $3640\text{ cm}^{-1}$  for MFM-300(Al) and MFM-300(Cr), respectively. In MFM-300(Al), upon increasing the  $CO_2$  partial pressures to 1.0 bar, the Al-O(H)-Al band centred at  $3690\text{ cm}^{-1}$  gradually decreases in intensity with a new band growing at  $3683\text{ cm}^{-1}$  which is observable from 60%  $CO_2$  loading. This new

peak continues to increase in intensity on additional  $CO_2$  loading. The redshift of  $7\text{ cm}^{-1}$  is consistent with the  $\mu_2\text{-OH}$  site being increasingly occupied by  $CO_2$  and is consistent with the crystallographic study. In comparison, the  $\mu_2\text{-OH}$  peak observed at  $3640\text{ cm}^{-1}$  in MFM-300(Cr) undergoes a redshift of  $2\text{ cm}^{-1}$  upon increasing  $CO_2$  loading and a significant increase in absorbance intensity. For MFM-300( $Al_{0.67}Cr_{0.33}$ ), distinct absorbance bands for the different  $\nu(OH)$  stretching modes were observed at  $3692$ ,  $3672$  and  $3644\text{ cm}^{-1}$  for Al-O(H)-Al, Al-O(H)-Cr and Cr-O(H)-Cr modes, respectively. Upon increasing  $CO_2$  partial pressures to 1 bar, the Al-OH-Al band centred at  $3692\text{ cm}^{-1}$  decreases in intensity and a new band at  $3683\text{ cm}^{-1}$  emerges. This indicates that the Al-O(H)-Al band is significantly affected by the presence of  $CO_2$ , suggesting a partial depletion of Al-O(H)-Al moieties in the material and  $CO_2$  binding to this moiety. The same is observed for Al-O(H)-Cr with a redshift of  $7\text{ cm}^{-1}$  to  $3665\text{ cm}^{-1}$ . A shift of  $2\text{ cm}^{-1}$  from  $3644$  to  $3642\text{ cm}^{-1}$  is observed in the Cr-O(H)-Cr mode along

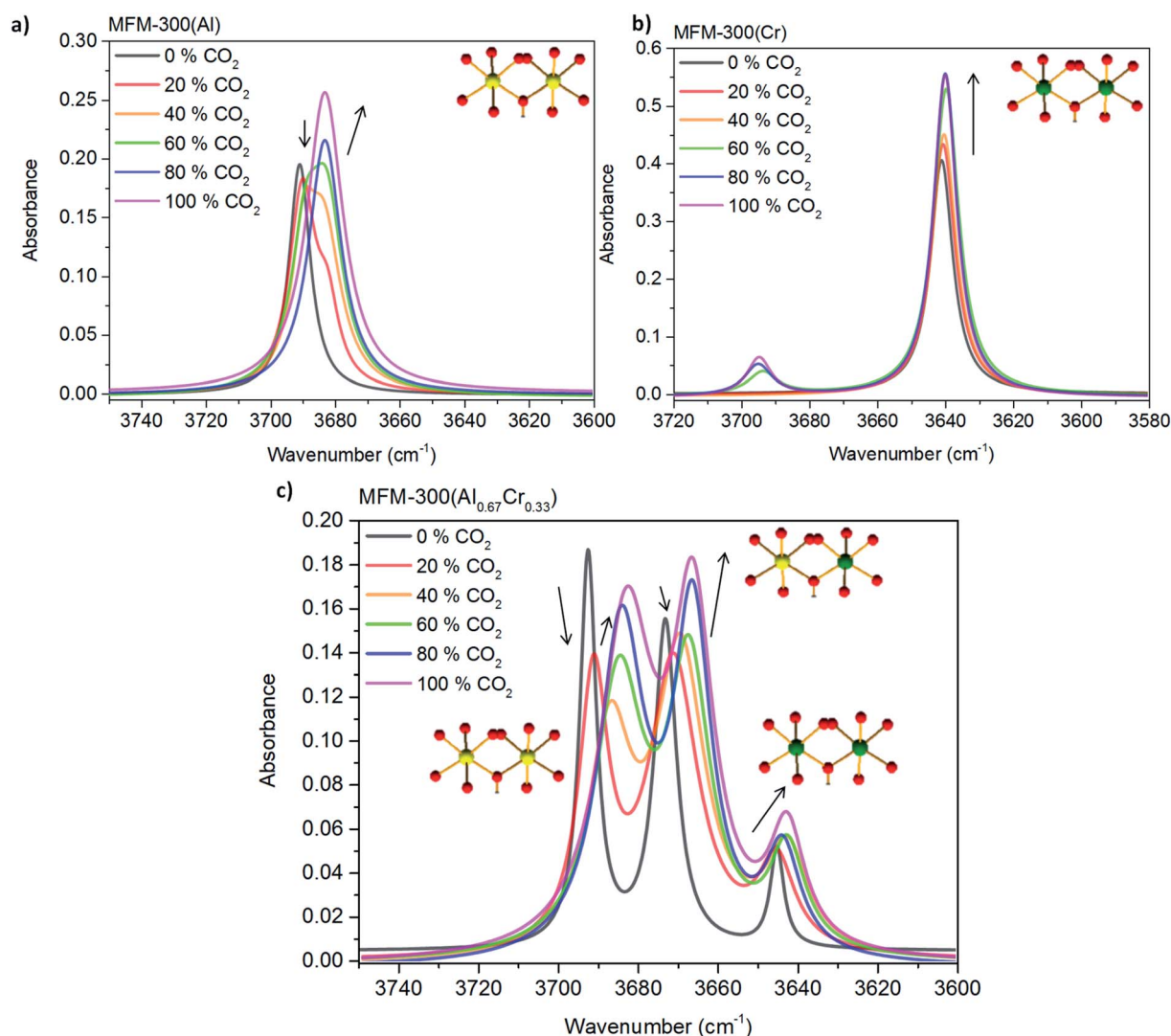


Fig. 6 FTIR spectra of the  $\nu(\mu_2\text{-OH})$  stretch region of (a) MFM-300(Al), (b) MFM-300(Cr), and (c) MFM-300( $Al_{0.67}Cr_{0.33}$ ) upon increasing  $CO_2$  loadings from 0 to 100%.



with a broadening of the peak. All  $\nu(\text{OH})$  stretching modes were found to shift to lower frequencies upon increasing  $\text{CO}_2$  loadings which suggests a weakening of the O–H bond in the metal-hydroxyl moiety consistent with the formation of  $\mu_2\text{-OH}\cdots\text{O}=\text{C}=\text{O}$  binding site.

## Conclusion

Stable MOFs show increasing promise in the application of capture of toxic gases.<sup>23</sup> The binding domains for  $\text{CO}_2$ ,  $\text{SO}_2$  and  $\text{C}_2\text{H}_2$  and their host-guest binding dynamics have been studied in a family of three iso-structural MOFs,  $\text{MFM-300}(\text{Al}_{1-x}\text{Cr}_x)$  ( $x = 0, 0.33, 1$ ) by *in situ* synchrotron X-ray diffraction and IR micro-spectroscopy. Both  $\text{MFM-300}(\text{Al}_{0.67}\text{Cr}_{0.33})$  and  $\text{MFM-300}(\text{Cr})$  show enhanced  $\text{CO}_2$ ,  $\text{C}_2\text{H}_2$  and  $\text{SO}_2$  adsorption uptake than  $\text{MFM-300}(\text{Al})$ .  $\text{MFM-300}(\text{Al}_{0.67}\text{Cr}_{0.33})$  exhibits the highest number of  $\text{CO}_2$ ,  $\text{C}_2\text{H}_2$  and  $\text{SO}_2$  molecules per metal compared with the homo-metallic analogues, which is likely due to the complex distribution of –OH sites within the pores and the formation of defects *via* doping of  $\text{MFM-300}(\text{Al})$  with  $\text{Cr}(\text{III})$  leading to increased porosity and additional binding and interaction sites.  $\text{MFM-300}(\text{Cr})$  shows the highest  $\text{SO}_2/\text{CO}_2$  IAST selectivity, which has also been confirmed by breakthrough experiments.  $\text{MFM-300}(\text{Cr})$  also promises excellent  $\text{SO}_2$  regenerability as confirmed by cycling measurements, demonstrating its potential for selective removal of  $\text{SO}_2$ .

## Conflicts of interest

The authors declare no competing financial interests.

## Acknowledgements

We thank EPSRC (EP/I011870) for support. This project has received funding from the European Research Council (ERC) under the European Union's Horizon 2020 research and innovation programme (grant agreement No 742401, NANOCHEM). We thank the Royal Society, Peking University and Universities of Nottingham and Manchester for funding. We thank Diamond Light Source for access to Beamlines B22 and I11.

## Notes and references

- 1 S. Yang, A. J. Ramirez-Cuesta, R. Newby, V. Garcia-Sakai, P. Manuel, S. K. Callear, S. I. Campbell, C. C. Tang and M. Schröder, *Nat. Chem.*, 2015, 7, 121–129.
- 2 S. Yang, J. Sun, A. J. Ramirez-Cuesta, S. K. Callear, W. I. F. David, D. P. Anderson, R. Newby, A. J. Blake, J. E. Parker, C. C. Tang and M. Schröder, *Nat. Chem.*, 2012, 4, 887–894.
- 3 J. Yang, X. Yan, T. Xue and Y. Liu, *RSC Adv.*, 2016, 6, 55266–55271.
- 4 G. E. Cmarik, M. Kim, S. M. Cohen and K. S. Walton, *Langmuir*, 2012, 28, 15606–15613.
- 5 R. Vaidhyanathan, S. S. Iremonger, G. K. H. Shimizu, P. G. Boyd, S. Alavi and T. K. Woo, *Science*, 2010, 330, 650–653.
- 6 S. Noro and T. Nakamura, *NPG Asia Mater.*, 2017, 9, e433.
- 7 H. Deng, C. J. Doonan, H. Furukawa, R. B. Ferreira, J. Towne, C. B. Knobler, B. Wang and O. M. Yaghi, *Science*, 2010, 327, 846–850.
- 8 Y. Yuan, J. Li, X. Sun, G. Li, Y. Liu, G. Verma and S. Ma, *Chem. Mater.*, 2019, 31, 1084–1091.
- 9 X. Lin, I. Telepeni, A. J. Blake, A. Dailly, C. M. Brown, J. M. Simmons, M. Zoppi, G. S. Walker, K. M. Thomas, T. J. Mays, P. Hubberstey, N. R. Champness and M. Schröder, *J. Am. Chem. Soc.*, 2009, 131, 2159–2171.
- 10 J. Zhang, S. Yao, S. Liu, B. Liu, X. Sun, B. Zheng, G. Li, Y. Li, Q. Huo and Y. Liu, *Cryst. Growth Des.*, 2017, 17, 2131–2139.
- 11 Y. P. He, Y. X. Tan and J. Zhang, *Cryst. Growth Des.*, 2013, 13, 6–9.
- 12 T. L. Easun, F. Moreau, Y. Yan, S. Yang and M. Schröder, *Chem. Soc. Rev.*, 2017, 46, 239–274.
- 13 T. Islamoglu, D. Ray, P. Li, M. B. Majewski, I. Akpınar, X. Zhang, C. J. Cramer, L. Gagliardi and O. K. Farha, *Inorg. Chem.*, 2018, 57, 13246–13251.
- 14 Q. Guo, L. Ren, P. Kumar, V. J. Cybulskis, K. A. Mkhoyan, M. E. Davis and M. Tsapatsis, *Angew. Chem., Int. Ed.*, 2018, 57, 4926–4930.
- 15 G. Férey, C. Mellot-Draznieks, C. Serre and F. Millange, *Science*, 2005, 309, 2040–2042.
- 16 Y. K. Hwang, D. Y. Hong, J. S. Chang, S. H. Jhung, Y. K. Seo, J. Kim, A. Vimont, M. Daturi, C. Serre and G. Férey, *Angew. Chem., Int. Ed.*, 2008, 47, 4144–4148.
- 17 A. Herbst, A. Khutia and C. Janiak, *Inorg. Chem.*, 2014, 53, 7319–7333.
- 18 X. Lian, D. Feng, Y.-P. Chen and H. Zhou, *Chem. Sci.*, 2015, 6, 7044–7048.
- 19 I. J. Kang, N. A. Khan, E. Haque and S. H. Jhung, *Chem.–Eur. J.*, 2011, 17, 6437–6442.
- 20 D. Sun, F. Sun, X. Deng and Z. Li, *Inorg. Chem.*, 2015, 54, 8639–8643.
- 21 C. P. Krap, S. Yang, R. Newby, A. Dhakshinamoorthy, H. García, I. Cebula, T. L. Easun, M. Savage, J. E. Eyley, S. Gao, A. J. Blake, W. Lewis, P. H. Beton, M. R. Warren, D. R. Allan, M. D. Frogley, C. C. Tang and M. Schröder, *Inorg. Chem.*, 2016, 55, 1076–1088.
- 22 J. M. P. A. L. Myers, *AIChE J.*, 1964, 11, 121–127.
- 23 X. Han, S. Yang and M. Schröder, *Nat. Rev. Chem.*, 2019, 3, 108–118.
- 24 M. Savage, Y. Cheng, T. L. Easun, J. E. Eyley, S. P. Argent, M. R. Warren, W. Lewis, C. Murray, C. C. Tang, M. D. Frogley, R. T. Murden, M. J. Benham, A. N. Fitch, A. J. Blake, A. J. Ramirez-Cuesta, S. Yang and M. Schröder, *Adv. Mater.*, 2016, 28, 8705–8711.
- 25 D. Z. Yang, M. Q. Hou, H. Ning, J. Ma, X. C. Kang, J. L. Zhang and B. X. Han, *ChenSusChem*, 2013, 7, 1191–1195.
- 26 J.-Y. Lee, T. C. Keener and Y. J. Yang, *J. Air Waste Manage. Assoc.*, 2009, 59, 725–732.
- 27 J. Yu and P. B. Balbuena, *ACS Sustainable Chem. Eng.*, 2015, 3, 117–124.
- 28 Z. Lu, H. G. W. Godfrey, I. Silva, Y. Cheng, M. Savage, F. Tuna, E. J. L. McInnes, S. J. Teat, K. J. Gagnon,



## Paper

M. D. Frogley, P. Manuel, S. Rudic, A. J. Ramirez-Cuesta, S. Yang and M. Schröder, *Nat. Commun.*, 2017, **8**, 14212.  
29 M. Savage, Y. Cheng, T. L. Easun, J. E. Eyley, S. P. Argent, M. R. Warren, W. Lewis, C. Murray, C. C. Tang,

M. D. Frogley, R. T. Murden, M. J. Benham, A. N. Fitch, A. J. Blake, A. J. Ramirez-Cuesta, S. Yang and M. Schröder, *Adv. Mater.*, 2016, **28**, 8705–8711.

